SUPPLEMENTARY INFORMATION

Cryo-EM structure of the *E. coli* translating ribosome in complex with SRP and its receptor

Leandro F. Estrozi [1,2,5], Daniel Boehringer[3,5], Shu-ou Shan[4], Nenad Ban[3]* & Christiane Schaffitzel[1,2]*

[1] European Molecular Biology Laboratory, Grenoble Outstation, 6 Rue Jules Horowitz, BP181, 38042 Grenoble Cedex 9, France
[2] Unit of Virus Host-Cell Interactions, UJF-EMBL-CNRS, UMI 3265, 6 Rue Jules Horowitz, 38042 Grenoble Cedex 9, France
[3] ETH Zurich, Institute of Molecular Biology and Biophysics, Schafmattstr. 20, 8093 Zurich, Switzerland.
[4] Division of Chemistry and Chemical Engineering, California Institute of Technology, 1200 E. California Blvd, Pasadena, CA 91125, United States
[5] these authors contributed equally
* Corresponding authors: ban@mol.biol.ethz.ch, schaffitzel@embl.fr

SUPPLEMENTARY METHODS

scSRP Cloning, Expression and Purification.

Full-length FtsY was PCR amplified from pET24a-FtsY (derived from pET9-FtsY[1]) using oligonucleotides pET24aXbaIfor (5'-CAATTCCCCTCTAGAAATAATTTTGTTTAAC-3'), linker1ftsYrev (5'-ACCGCCGCCAGAACCGCCACCTCCTGAGCTATCCTCTCGGG CAAAAAGTG-3'), linker2ftsYrev (5'-CCACCACCGCCAGAACCACCGCCACCGCTCCCAC CGCCGCCAGAACCG-3') and linker3ftsYrev (5'-TTGCATGAAGCTTTGCATGGGTACCGCC TCCGCCGGAACCACCACCGCCAGAACC-3'). The PCR product was *Xba*I/*Hin*dIII-digested and ligated into *Xba*I/*Hin*dIII-digested pET24a (Novagen, Madison, WI, USA) yielding pET24ftsYlinkerKpnI. Ffh was amplified by PCR from pET24aFfh[2] using oligonucleotides FfhKpnIfor (5'-CATGCATGGGTACCATGTTTGATAATTTAACCGATCG-3') and FfhHindIIIrev (5'-GAGTGCGGCCGCAAGCTTAGTGATGGTGATG-3'). The Ffh PCR product was *Kpn*I/*Hin*dIII-digested and ligated into *Kpn*I/*Hin*dIII-digested pET24ftsYlinkerKpnI yielding pET24aFtsYlinkFfh. This plasmid encodes full-length FtsY and full-length Ffh with a C-terminal His6-tag. The FtsY C-terminus is covalently linked to the Ffh N-terminus via a 31-amino acid glycine-serine-rich linker.

pET24aFtsYlinkFfh and pUC19Ffs[3] were transformed in BL21Star(DE3) (Invitrogen, Carlsbad, CA, USA) and grown in dYT medium at 30ºC. The cultures were induced at an OD(600 nm) of 1.1 with 1 mM IPTG and harvested after 6 hours. The cells were resuspended in Buffer A (50 mM Hepes-KOH, 100 mM KCl, 10 mM $MgCl_2$, 10 mM imidazole, 1 mM β-mercaptoethanol, 0.1 mM TritonX-1000, 0.1 mM PMSF, pH 8.0) and lysed by two passages through an Emulsiflex C5 Cell Cracker (Avestin, Ottawa, Canada). The cleared lysate (SS34 rotor, 19000 rpm, 30 min, 4 ºC) was loaded onto a HisTrap column (GE Healthcare, UK) equilibrated with Buffer A. The column was washed with high-salt buffer (50 mM Hepes-KOH, 500 mM KCl, 10 mM $MgCl_2$, 10 mM imidazole, 1 mM β-mercaptoethanol, 0.1 mM TritonX-100, pH 8.0) and the scSRP was eluted with Buffer B (50 mM Hepes-KOH pH 8.0, 100 mM KCl, 10 mM $MgCl_2$, 125 mM imidazole, 1 mM β-mercaptoethanol, 0.1 mM TritonX-100). The eluate was diluted 1:5 into Ionex-Buffer A (50 mM Hepes-KOH, 60 mM KCl, 10 mM $MgCl_2$, 1 mM EDTA, 1 mM DTT, pH 7.5) and loaded onto a MonoQ column (GE Healthcare, UK) equilibrated with Ionex Buffer A. scSRP eluted at approximately 600 mM KCl using a linear gradient from 0 to 100% Ionex-Buffer B (50 mM Hepes-KOH, 1 M KCl, 10 mM $MgCl_2$, 1 mM EDTA, 1 mM DTT, pH 7.5). scSRP containing fractions were pooled, diluted into buffer FY (50 mM Hepes-KOH, 100 mM KOAc, 8 mM $Mg(OAc)_2$, pH

7.5), concentrated with a Vivaspin concentrator YM-10 (Vivascience, Stonehouse, UK) and frozen in liquid nitrogen.

Preparation of Ribosome-Nascent Chain (RNC) Complexes.

pUC19StrepFtsQSecM was transcribed and translated *in vitro* as described[4]. RNCs were purified by affinity chromatography and sucrose gradient centrifugation[4]. The RNCs were dissolved in Buffer FY.

GTPase Assays.

All GTPase assays were carried out at 25°C in SRP buffer (50 mM HEPES-KOH, pH 7.5, 150 mM KOAc, 10 mM $Mg(OAc)_2$, 2 mM DTT, 0.01% Nikkol). 50 nM scSRP was incubated with or without 260 nM RNC, and the reaction was initiated by the addition of 100 µM GTP doped with γ-32P-GTP. The GTPase reaction with unlinked SRP and FtsY were carried out with 50 nM SRP, saturating FtsY (20 µM), and 100 µM GTP with or without 150 –160 nM RNC.

Grid Preparation, Electron Microscopy and Image Analysis.

120 nM RNCs were incubated with a 15-fold molar excess of purified scSRP for 10 min at 30°C. Subsequently, 3 µl sample (120 nM RNCs) were applied to glow-discharged carbon-coated lacey formvar grids (300 mesh, Ted Pella) followed by manual blotting and plunging into a liquid ethane bath. Grids were imaged in a FEI F20 electron microscope (FEI, Hillsboro, OR) operated at an accelerating voltage of 200 kV. Images were recorded at a magnification of 50,000x under low dose conditions at 1.5-3.5 µm defocus on Kodak SO-163 film (Eastman Kodak, Rochester, NY). The images were scanned with a Nikon super coolscan 9000 scanner, corresponding to a pixel size of 1.27 Å on the object scale. The data were binned to 3.81 Å/pixel. 93,535 particles were picked semi-automatically using Boxer[5] and corrected for CTF using Bsoft[6] based on CTF parameters estimated by CTFFIND[7]. An initial structure of the scSRP-RNC complex was determined using a low-pass-filtered vacant RNC as an initial reference[3].

Multi-Particle Refinement.

In the initial structure, density at the tunnel exit could be attributed to scSRP. However, this initial density for scSRP was weak, showing a fragmented appearance at the threshold level used to display the ribosome. This indicates substoichiometric binding or conformational heterogeneity. To investigate this heterogeneity, we used a multi-particle refinement strategy for unsupervised classification of the dataset[8] (Supplementary Fig.2). The dataset was split into subsets using a vacant 70S *Escherichia coli* ribosome as an additional reference with Imagic-5[9]. The structure of the vacant 70S ribosome was calculated using a

dataset obtained from a preparation of tight-coupled 70S *E. coli* ribosomes[10] as described previously[11]. In the first sorting step the dataset was split into two subpopulations using the initial structure of the scSRP-RNC complex and the vacant 70S ribosome as references. This sorting step was repeated using the resulting two structures as new references, until a stable subpopulation of images were assigned to each reference. In the subsequent sorting step, the two resulting 3D structures and a vacant 70S ribosome were used as new references to obtain three subpopulations. The resulting three structures showed tRNA containing ribosomes in the non-ratcheted (class1) and ratcheted (class2) conformation and an empty non-ratcheted ribosome. The non-ratcheted ribosome structure with a stably bound P-site tRNA (class1) showed strong density at the tunnel exit for scSRP (Supplementary Fig.2). This class1 of ribosomes was used for further refinement to higher resolution using Spider[12].

The resolution of the final reconstruction (28,822 particles) was assessed by Fourier shell correlation 0.5 criterion to be 13.5Å (10Å according to FSC 0.143 criterion[13], Supplementary Fig.3).

Generation of the Atomic Model.

The *E. coli* 70S ribosome atomic model[14] was fitted as a rigid body using the program URO[15]. The atomic model of the *E. coli* SRP-FtsY complex was generated manually using the complex of the M-domain with RNA domain IV of *E. coli*[16], the 3D model for the complete *E. coli* 4.5S RNA from the SRP database[17], the crystal structure of the Ffh NG domain and the structure of the FtsY NG domain (1OKK.pdb)[18]. The model was energy minimized using CNS Version1.1[19].

SUPPLEMENTARY DISCUSSION

Single-chain SRP (scSRP) Construct Design.

The distance between the FtsY C terminus (residue 303, *Thermus aquaticus* numbering) and the N terminus of Ffh (residue 4, *Th. aquaticus* numbering) in the *early* state is 34 Å in our quasi-atomic model and 36 Å in the crystal structure of the *closed-activated* state which was used to estimate the required linker length[18]. The distance between the C-terminus of FtsY in the present model and the N terminus of Ffh in the RNC-SRP model[20] (Ffh4 –FtsY303) is 42Å.

In our single-chain construct, 36 amino acid residues are linking FtsY residue 303 and Ffh residue 4 (31-residue glycine-serine linker and 5 unordered residues that are not visible in the crystal structure [18]). The maximal distance that could be bridged by these amino acids is 125 Å. Thus, this linker should be able to encompass the N domain of Ffh, should not interfere with FtsY binding and should not influence the relative positioning of the Ffh-FtsY NG domains. This is supported by several lines of evidence: (i) the scSRP construct is not toxic when overexpressed in *E. coli*. (ii) The activity of scSRP was similar to that of the wildtype SRP and FtsY (unlinked factors) (Fig. 1; Supplementary Fig.1). (iii) The distance between the Ffh-FtsY N domains in the *early* model (34 Å) is similar to the distance observed in the crystal structures of the *closed-activated* complex (36 Å).

Rationale for the Placement of the FtsY and Ffh NG Domains.

The 4.5S RNA part of the SRP density[3,20] superimposes with the RNA part in the scSRP construct (Supplementary Fig. 4). The bilobal density at the tunnel exit above ribosomal protein L23 and L29 can be attributed to the highly homologous NG-domains of Ffh and FtsY. Based on the arrangement of Ffh and FtsY in the crystal structure of Ffh-FtsY heterodimer[18,21] in the presence of non-hydrolysable GTP, two conformations are possible: The conformation as shown in Fig. 2 and an alternative conformation with the Ffh and FtsY NG-domains flipped around by 180 degree.

Several lines of evidence suggest that the lobe above L23 can be assigned to Ffh. The alternative positioning is less likely as the 41-residue linker between the Ffh NG and M domains (a) would point to the membrane and (b) would have to completely unfold. In case of the alternative positioning, the linker would have to span a distance of ~75 Å (in comparison to 30 Å in the RNC-SRP model [20] and ~49 Å in our *early* model). The linker would have to wrap around the NG-domains in order to not overlap with the Ffh-FtsY NG-

domain interface. Fitting of the Ffh and FtsY NG-domains as shown in Fig. 2, requires the least measure of rearrangements of the Ffh conformation compared to the Ffh conformation in the SRP-RNC complex observed by electron microscopy [20] and by Fluorescence Resonance Energy Transfer (FRET) [22]. Superimposing the Ffh-NG domain onto the density of the scSRP-RNC complex shows that the G-domain of Ffh fits into the density lobe above L23 and only small rearrangements are required to fit the Ffh N-domain into the density (Supplementary Fig. 4 a,b).

The placement of FtsY near the 4.5S RNA tetraloop is consistent with biochemical evidence showing that FtsY interacts directly with the SRP RNA tetraloop: (i) Mutations in the 4.5S RNA tetraloop abolish SRP-FtsY interactions without affecting the Ffh - 4.5S RNA interaction [2,23]. (ii) Mutation of a highly conserved basic residue in the FtsY G domain (Lys399) abolishes the 4.5S RNA-mediated acceleration of SRP-FtsY complex assembly [24]. (iii) Combination of the Lys399 and 4.5S RNA tetraloop mutation does not cause additional defects indicating that both mutations disrupt the 4.5S RNA-FtsY interaction [24]. (iv) Both the tetraloop and the Lys399 mutation affect the stability of the *early* state (visualized in this study) [24]. (v) Lys399 is conserved in all the cytosolic SRP receptors whose function is dependent on the SRP RNA, but is changed to uncharged residues in a RNA-less chloroplast SRP pathway [24]. Mutation of the corresponding alanine back to lysine in chloroplast FtsY restored the ability of the SRP RNA to stimulate the Ffh-cpFtsY interaction.

Flexibility of the SRP-FtsY part

We observe an ellipsoidal cross-section of the SRP RNA part which could be caused by structural flexibility of the scSRP or preferred orientation of the images. Our reconstruction includes all views (angular distribution shown in Supplementary Fig. 3b) and in fact, we do not observe ellipticity of the ribosomal RNA helices. A certain degree of rotational flexibility in the SRP-FtsY which has a single connection to the large ribosomal subunit can give rise to an elliptic cross-section of the SRP RNA and to a somewhat lower resolution of the scSRP of 18.5Å compared to the ribosome part (13 Å, FSC=0.5) (Supplementary Fig. 3a).

SUPPLEMENTARY FIGURES

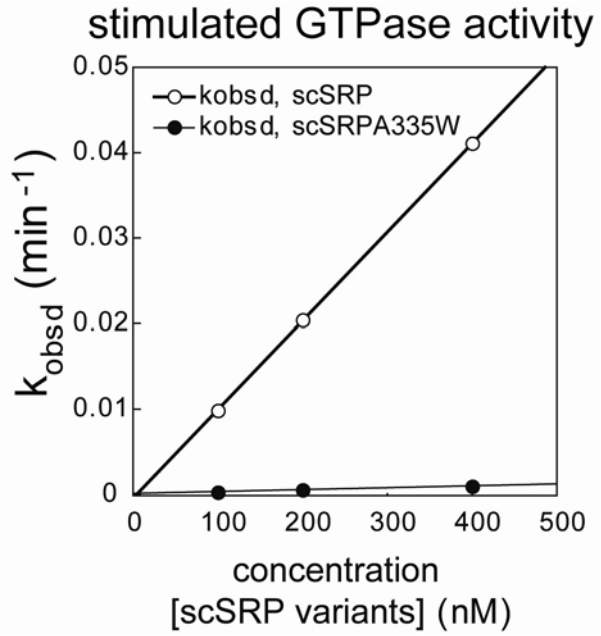

Supplementary Figure 1. Activity Assay of scSRP. The FtsY Ala335Trp mutation in scSRPmut inhibits the GTPase activity of the scSRP by 50-fold, consistent with results obtained with the unlinked complex [25].

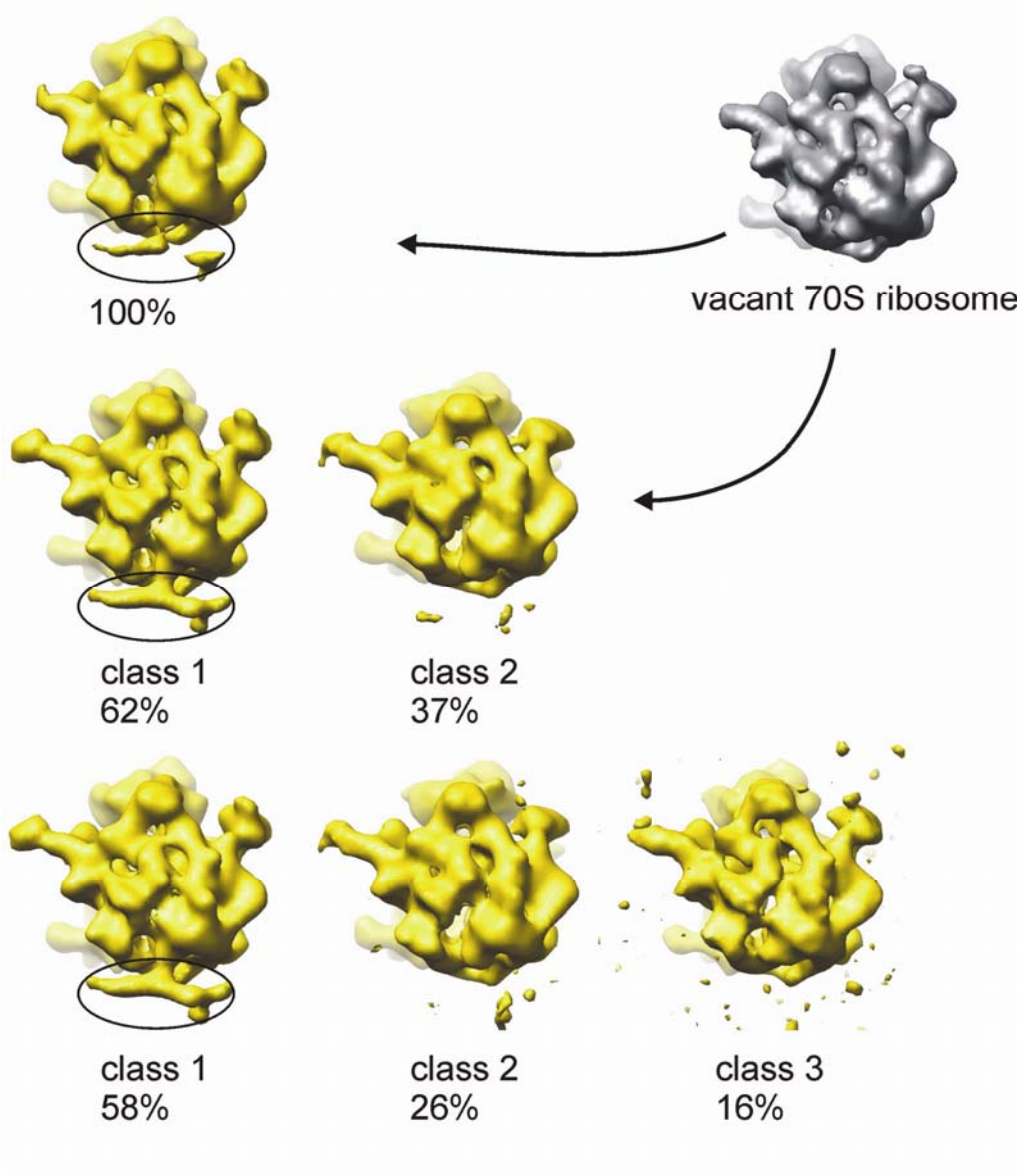

Supplementary Figure 2. Multi-Particle Refinement. The initial reconstruction of the RNC-scSRP complex showed only weak density for scSRP (circle) at the ribosomal tunnel exit (top). To obtain homogenous particle subgroups a multi-particle refinement strategy was employed [8]. To select for RNCs with bound scSRP, the structure of tight-coupled 70S *E. coli* ribosomes [10] was used as a second reference (top right, colored grey) resulting in two volumes with and without scSRP density (second row). Reference projections of both volumes were used to sort the dataset by cross-correlation. In a third round, the two resulting structures (class 1 and class 2) and the tight-coupled 70S ribosome (top in grey) were used as reference volumes resulting in three structures (bottom) that contained tRNA in the non-ratcheted conformation with scSRP bound (class 1) and ratcheted conformation (class 2) as well as an empty non-ratcheted ribosome (class 3). Class 2 and 3 do not display scSRP density at the exit of the ribosomal tunnel.

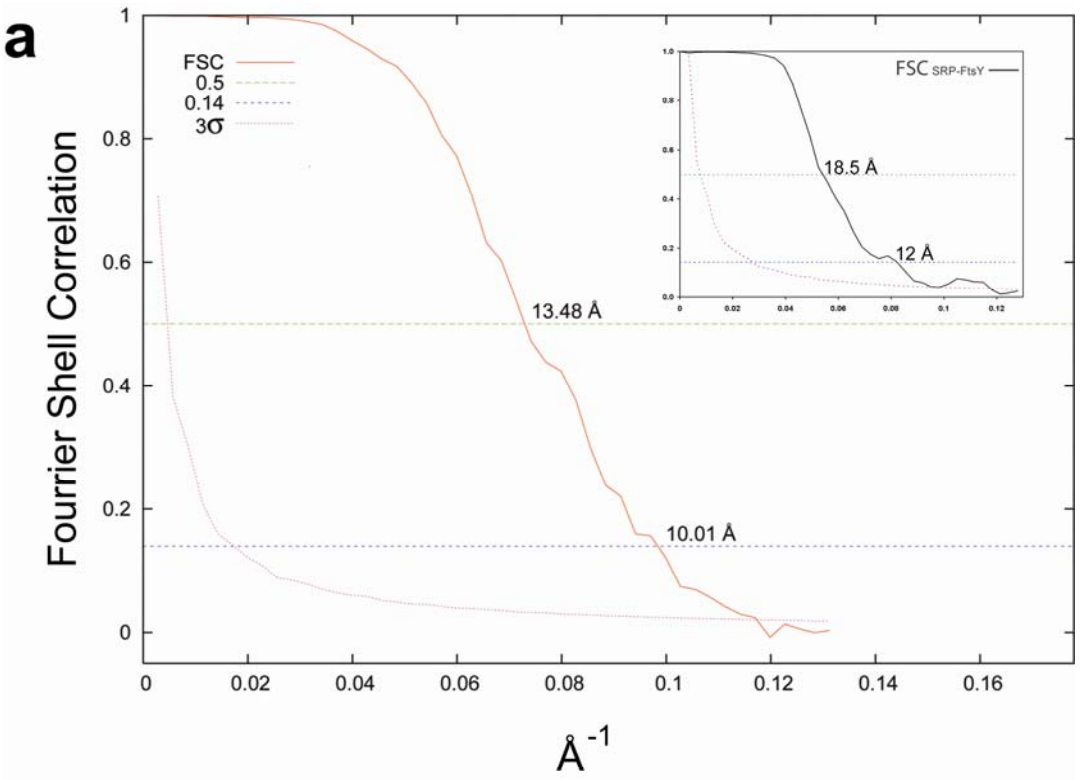

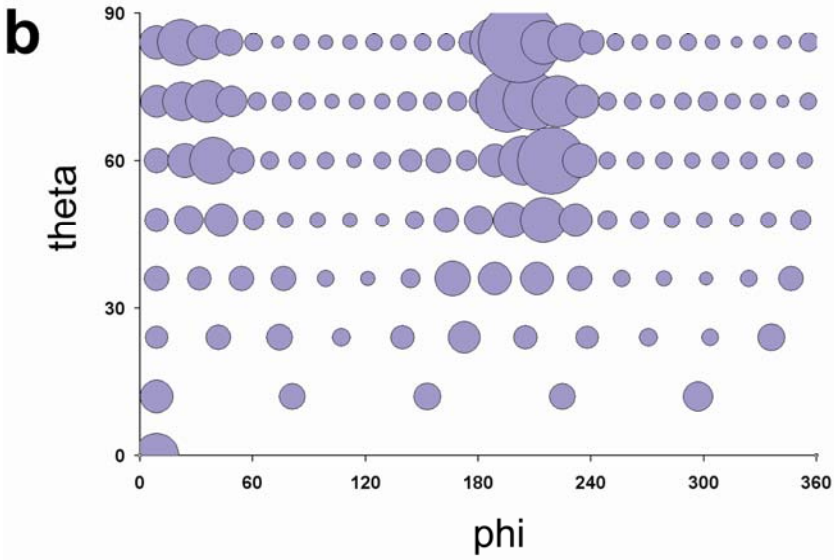

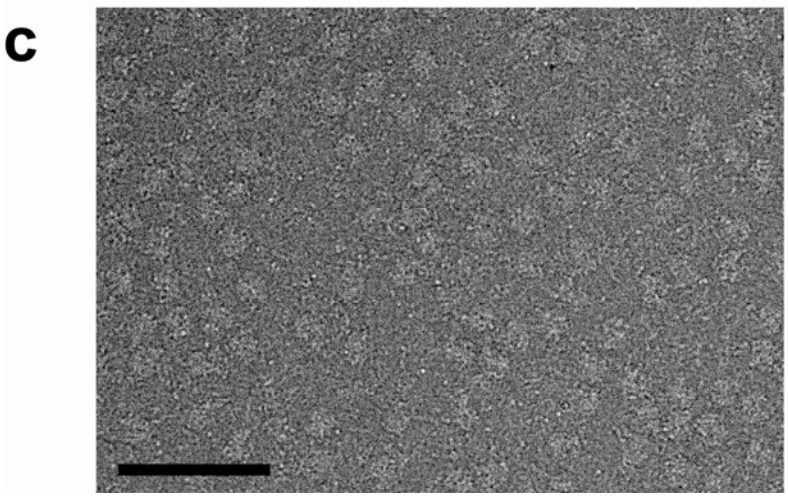

Nature Structural & Molecular Biology: doi:10.1038/nsmb.1952

Supplementary Figure 3. Resolution and Angular Distribution of the RNC-scSRP Reconstruction and Raw Data. (a) Diagram of the FSC function computed between two independent three-dimensional reconstructions of the RNC-scSRP complex (continuous red line). A set of 28,822 particles was randomly split in two half sets to calculate the 2 reconstructions. FSC=0.5 (dotted green line) indicates 13 Å resolution; and 10 Å according to the FSC=0.143 criterion (dotted blue line) [13]. **Inset:** FSC curve for the SRP-FtsY part without the ribosome. FSC=0.5 (black line) indicates an average resolution of 18.5 Å. **(b)** Map of angular distribution of the images used for the final reconstruction. The angular reference groups are represented by small circles. The areas of these circles are proportional to numbers of particle projections with that direction. **(c)** Scanned image of the RNC-scSRP sample in vitreous ice. The scale bar is 100 nm.

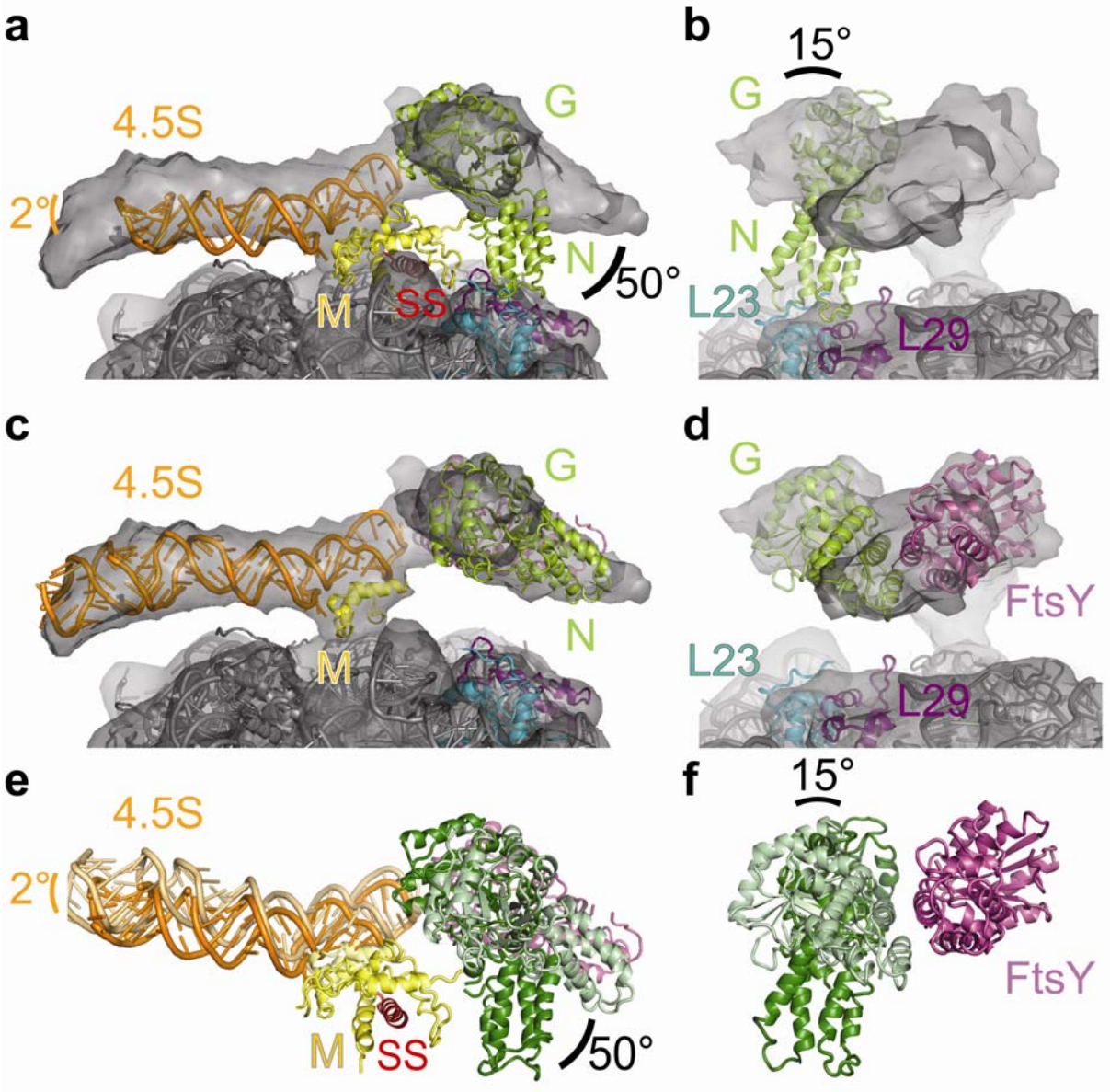

Supplementary Figure 4. **Conformational pre-organization of SRP by the ribosome for FtsY docking. (a,b)** Atomic model of *E. coli* SRP bound to the translating ribosome (PDB ID: 2J28)[20] placed into the density of the *early* conformation of the RNC-SRP-FtsY complex (shown in transparent grey). Conformational changes of the SRP during *early* complex formation are indicated. **(c,d)** Atomic model of the *early* SRP-FtsY complex (this study) placed into the density of the RNC-SRP-FtsY complex (ribosome model as in a,b) for comparison. **(e,f)** Overlay of the atomic models of SRP only (dark colors) and of SRP-FtsY in the *early* conformation (light colors). Same view as in the panels above. The 4.5S RNA is less kinked in the *early* RNC-SRP-FtsY complex and not connected to the ribosomal protein L32 as previously observed in the RNC-SRP structure [3,20]. Part of the density that accommodated the M domain and signal sequence in the RNC-SRP structure is not visible in the RNC-SRP-FtsY structure. rRNA and ribosomal proteins are depicted in grey, ribosomal protein L23 in cyan, L29 in purple, 4.5S RNA in orange, Ffh M domain in yellow, Ffh NG domain in green, the model of the signal anchor sequence in red, and the FtsY NG domain in magenta.

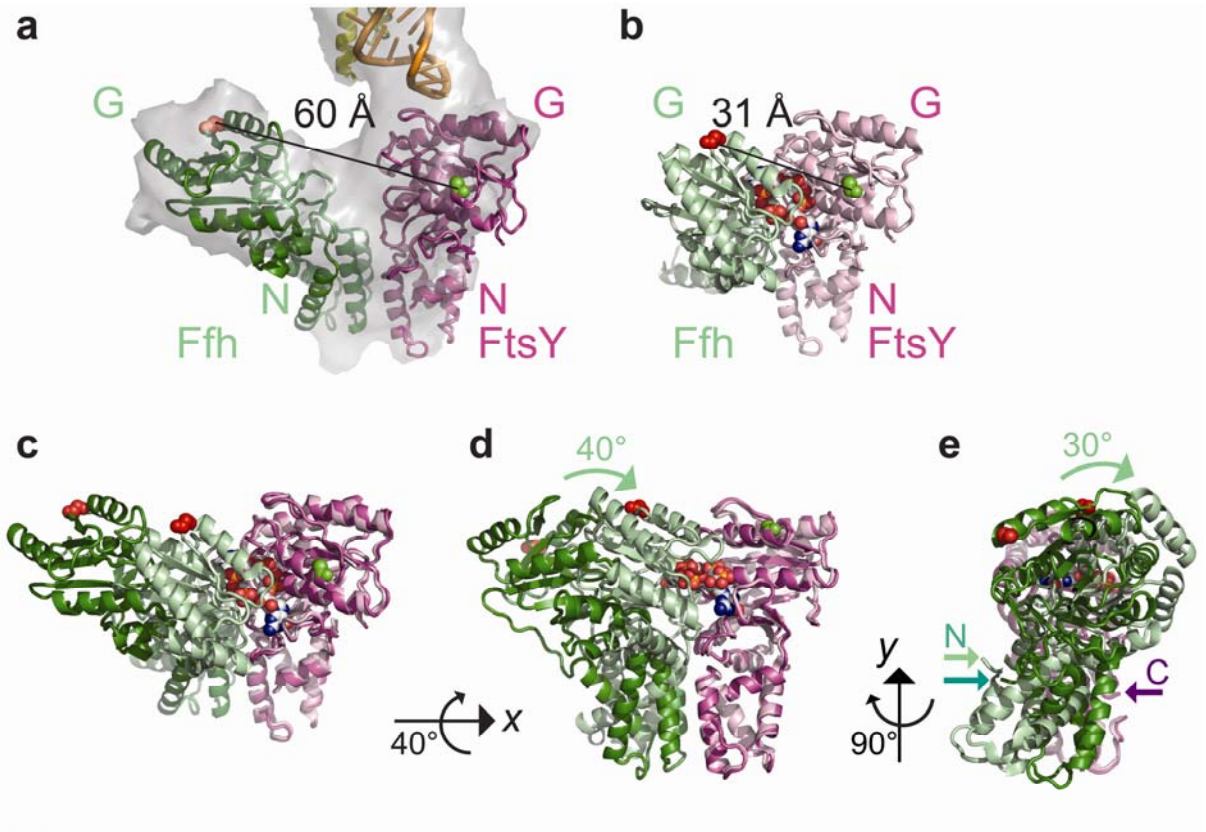

Supplementary Figure 5. **Position of the NG domains in the *early* and the *closed-activated* state of the Ffh-FtsY complex. (a)** Atomic model of the NG domains in the *early* state without nucleotide with the density of the *early* conformation of the RNC-SRP-FtsY complex (shown in transparent grey). The distance between Ffh153 (red spheres) and FtsY345 (green spheres) is ~ 60 Å. These residues were labeled in FRET experiments [26] resulting in a low FRET value for the *early* state. **(b)** Co-crystal structure of the NG domains representing the *closed-activated* state with non-hydrolysable GTP bound in the active site (sphere representation) [18,21] (PDB ID: 1OKK). The distance between the residues labeled for FRET experiments is 31 Å, in agreement with the high FRET value observed in the *closed* state [26]. **(c,d,e)** Overlay of the *early* and *closed-activated* state of the Ffh-FtsY complex. The FtsY NG domains were aligned, thus showing the required movement of the Ffh NG domain to form the *closed-activated* state with a strong NG domain interface. The arrow and degree of rotation indicates the relationship between the views. **(c)** Same view as in **a,b**. **(e)** The FtsY C-terminus and the Ffh N-termini are marked by arrows. The distance to be spanned by the linker is 34 Å in the *early* state and 36 Å in the *closed-activated* state. The Ffh NG domain is depicted in green (*early* state) and in palegreen (*closed-activated* state); FtsY NG domains are magenta (*early* state) and lightpink (*closed-activated* state).

SUPPLEMENTARY REFERENCES

1. Luirink, J. et al. An alternative protein targeting pathway in *Escherichia coli*: studies on the role of FtsY. *EMBO J.* **13**, 2289-2296 (1994).
2. Jagath, J.R. et al. Important role of the tetraloop region of 4.5S RNA in SRP binding to its receptor FtsY. *RNA* **7**, 293-301 (2001).
3. Schaffitzel, C. et al. Structure of the *E. coli* signal recognition particle bound to a translating ribosome. *Nature* **444**, 503-506 (2006).
4. Schaffitzel, C. & Ban, N. Generation of ribosome nascent chain complexes for structural and functional studies. *J. Struct. Biol.* **158**, 463-471 (2007).
5. Ludtke, S.J., Baldwin, P.R. & Chiu, W. EMAN: semiautomated software for high-resolution single-particle reconstructions. *J. Struct. Biol.* **128**, 82-97 (1999).
6. Heymann, J.B. & Belnap, D.M. Bsoft: image processing and molecular modeling for electron microscopy. *J. Struct. Biol.* **157**, 3-18 (2007).
7. Mindell, J.A. & Grigorieff, N. Accurate determination of local defocus and specimen tilt in electron microscopy. *J. Struct. Biol.* **142**, 334-347 (2003).
8. Connell, S.R. et al. A new tRNA intermediate revealed on the ribosome during EF4-mediated back-translocation. *Nat. Struct. Mol. Biol.* **15**, 910-915 (2008).
9. van Heel, M., Harauz, G., Orlova, E.V., Schmidt, R. & Schatz, M. A new generation of the IMAGIC image processing system. *J. Struct. Biol.* **116**, 17-24 (1996).
10. Bingel-Erlenmeyer, R. et al. A peptide deformylase-ribosome complex reveals mechanism of nascent chain processing. *Nature* **452**, 108-111 (2008).
11. Kohler, R. et al. YidC and Oxa1 form dimeric insertion pores on the translating ribosome. *Mol. Cell* **34**, 344-353 (2009).
12. Frank, J. et al. SPIDER and WEB: processing and visualization of images in 3D electron microscopy and related fields. *J. Struct. Biol.* **116**, 190-199 (1996).
13. Rosenthal, P.B. & Henderson, R. Optimal determination of particle orientation, absolute hand, and contrast loss in single-particle electron cryomicroscopy. *J. Mol. Biol.* **333**, 721-745 (2003).
14. Schuwirth, B.S. et al. Structures of the bacterial ribosome at 3.5 Å resolution. *Science* **310**, 827-834 (2005).
15. Navaza, J., Lepault, J., Rey, F.A., Alvarez-Rua, C. & Borge, J. On the fitting of model electron densities into EM reconstructions: a reciprocal-space formulation. *Acta Crystallogr. D Biol. Crystallogr.* **58**, 1820-1825 (2002).
16. Batey, R.T., Rambo, R.P., Lucast, L., Rha, B. & Doudna, J.A. Crystal structure of the ribonucleoprotein core of the signal recognition particle. *Science* **287**, 1232-1239 (2000).
17. Andersen, E.S. et al. The tmRDB and SRPDB resources. *Nucleic Acids Res.* **34**, D163-168 (2006).
18. Focia, P.J., Shepotinovskaya, I.V., Seidler, J.A. & Freymann, D.M. Heterodimeric GTPase core of the SRP targeting complex. *Science* **303**, 373-377 (2004).
19. Brunger, A.T. et al. Crystallography & NMR system: A new software suite for macromolecular structure determination. *Acta Crystallogr. D Biol. Crystallogr.* **54**, 905-921 (1998).
20. Halic, M. et al. Following the signal sequence from ribosomal tunnel exit to signal recognition particle. *Nature* **444**, 507-511 (2006).
21. Egea, P.F. et al. Substrate twinning activates the signal recognition particle and its receptor. *Nature* **427**, 215-221 (2004).

22. Buskiewicz, I.A., Jöckel, J., Rodnina, M.V. & Wintermeyer, W. Conformation of the signal recognition particle in ribosomal targeting complexes. *RNA* **15**, 44-54 (2009).
23. Siu, F.Y., Spanggord, R.J. & Doudna, J.A. SRP RNA provides the physiologically essential GTPase activation function in cotranslational protein targeting. *RNA* **13**, 240-250 (2007).
24. Shen, K. & Shan, S.O. Transient tether between the SRP RNA and SRP receptor ensures efficient cargo delivery during cotranslational protein targeting. *Proc. Natl. Acad. Sci. USA* 107, 7698-7703 (2010).
25. Shan, S.O., Chandrasekar, S. & Walter, P. Conformational changes in the GTPase modules of the signal reception particle and its receptor drive initiation of protein translocation. *J. Cell Biol.* **178**, 611-620 (2007).
26. Zhang, X., Schaffitzel, C., Ban, N. & Shan, S.O. Multiple conformational switches in a GTPase complex control co-translational protein targeting. *Proc. Natl. Acad. Sci. U.S.A.* **106**, 1754-1759 (2009).